sciendo

Polish Journal of Chemical Technology, 26, 4, 114—122, 10.2478/pjct-2024-0047

Photophysical and biological studies on structurally modified chlorophenyl-substituted pyrazolone derivatives

Ahmed M. Naglah[1], Abdulrahman A. Almehizia[1], Maniyar A.K.[2], Vidyagayatri Marrakkur[3], Lohit Naik[4*]

[1]Department of Pharmaceutical Chemistry, College of Pharmacy, King Saud University, P.O. Box 2457, Riyadh 11451, Saudi Arabia
[2]Department of physics, Government First Grade College Hubballi- 580032. Karnataka, India
[3]Department of Chemistry, NMKRV College for Women, Bengaluru-560006, India
[4]Department of Physics, RNS Institute of Technology, Bengaluru, 560 098, Karnataka, India and an Affiliated to Visvesvaraya Technological University, Belagavi, Karnataka, India
[*]*Corresponding authors: e-mail:* lohitresearch@gmail.com; anaglah@ksu.edu.sa

In this study, chlorophenyl-substituted pyrazolone derivatives (5a–5c) were synthesized via the Baylis-Hillman acetate reaction. Comprehensive physicochemical characterization was conducted using ^{1}H-NMR, FT-IR, and mass spectroscopy. Density Functional Theory (DFT) calculations at the B3LYP/6-31(G) level was employed to optimize molecular geometries and investigate electronic properties, revealing predominantly planar structures, with notable deviations in the pyrazole group. The HOMO and LUMO analyses showed π-delocalization across the entire molecule, with charge-transfer transitions dominating the excited states. Global Chemical Reactivity Descriptors (GCRD), including chemical potential, hardness, and electrophilicity index, were used to assess molecular stability and reactivity, indicating the molecules' resistance to electron cloud deformation. Biological evaluations revealed exceptional antimicrobial and antifungal activities of the derivatives, with compound 5a demonstrating the highest efficacy against *S. aureus*, *E. coli*, *A. niger* and C. albicans. Furthermore, antiproliferative studies against HepG2 liver carcinoma cells showed that compound 5a exhibited superior anticancer activity (IC50 = 6 μg/mL), attributed to its structural features, such as chlorophenyl groups and a piperidin-4-one moiety. These moieties enhance the compound's lipophilicity, facilitating cell membrane penetration and ROS generation, which contribute to apoptosis and inhibition of cancer cell growth. The findings suggest that chlorophenyl-pyrazolone derivatives, particularly 5a, hold promise as potent candidates for antimicrobial and anticancer therapies, paving the way for further pharmaceutical development.

Keywords: Chlorophenyl-substituted pyrazolone, biological activity, HOMO-LUMO, Mulkin plot.

INTRODUCTION

Heterocyclic compounds are a unique class of highly valuable compounds, exhibiting a wide range of applications[1–2]. They are widely distributed in nature and play a significant role in metabolism, forming the structural nucleus of various natural products such as antibiotics, hormones, alkaloids, and vitamins[3–5]. Among heterocyclic compounds, nitrogen-containing heterocycles are prevalent and serve as a core framework in a diverse library of heterocycles, finding applications in natural and other scientific disciplines[6]. These nitrogen-containing heterocycles possess distinctive structural features and are commonly found in natural products[7–8].

Pyrazole derivatives are one notable family of nitrogen-substituted compounds that show a wide range of biological activities[9–14]. Another compound, bipyrazole, has garnered significant attention due to its diuretic, cytotoxic, and cardiovascular efficacy. Additionally, bipyrazole finds applications in the paint and photographic industries and the development of fireproof resins. Pyrazolone, characterized by an extra keto group and a 3-oxygenated derivative, serves as a crucial element in medications like phenylbutazone and metamizole sodium. These non-steroidal anti-inflammatory drugs are renowned for their effective pain relief and fever-reducing abilities[15–20]. Furthermore, the benzo-fused derivative of pyrazole, known as tetrahydroindazole, is well-recognized for its biological activity and is utilized against cancer and inflammation[20–21].

Based on the importance, chlorophenyl-substituted pyrazolone derivatives were synthesized and their In-vitro biological activity alongside their photophysical properties was studied.

MATERIALS AND METHODS

The chemical compounds used for the present studies were of high purity from Fischer, Merck, and Sigma Aldrich companies. The FT-IR, ^{1}H-NMR (400MHz, DMSO-d_6) and LCMS spectra were recorded in Nicolet-Impact-410 FT-IR spectrometer, Bruker AC-400F, Agilent 1200 series instrument spectrometer respectively. The Heraus CHN rapid analyzer was employed for conducting elemental analysis. All compounds demonstrated C, H, and N analyses that were within ± 0.4% of the expected values.

The structural and theoretical analyses of synthesized molecules were conducted using GaussView 5.0 and Gaussian 09 W software packages. The optimization of synthesized molecules geometry was initially performed via Density Functional Theory (DFT) employing the B3LYP functional and 6-311G basis set. Subsequently, various theoretical investigations were carried out, encompassing atomic charge distribution in the ground state, Time-Dependent DFT (TD-DFT) analysis in the excited state, thermodynamic properties, structural properties, and optical properties. The DFT method B3LYP/6-311G was utilized for these analyses. Additionally, frontier molecular orbital analysis of the molecule was conducted both in a vacuum and in a liquid phase environment.

Synthesis of chlorophenyl pyrazalone derivatives

The stepwise reactions used to create the desired target molecules are outlined in Scheme-1.

Synthesis of Compound (2): Compound (2) was synthesized by reacting a mixture of 1-(4-chlorophenyl) ethan-1-one and diethyl oxalate in the presence of Lithium bis(trimethylsilyl)amide (LiHMDS) in THF at 0°C for 30 minutes.

Synthesis of Compound (3): Using compound (2) (1 mmol) and (2,4-dichlorophenyl)hydrazine (1 mmol), the reaction was carried out in ethanol (100 ml) with acetic acid (10 ml). The mixture was refluxed overnight at 80 °C. After completion, the reaction mixture was concentrated to remove ethanol, neutralized using Na_2CO_3, and the precipitate was filtered, dried, and purified by recrystallization in ethanol.

Synthesis of Compound (4): To a solution of compound (3) (1 mmol) in THF (50 ml), methanol (15 ml), and water (20 ml), lithium hydroxide (1.2 mmol) was added at room temperature (RT), and the mixture was stirred overnight. After reaction completion, the mixture was concentrated to remove volatiles, and the resulting residue was dissolved in water (50 ml) and extracted with ethyl acetate (2 × 100 ml). The aqueous layer was acidified to pH ~5 using 1N HCl, and the combined organic layer was washed with water (50 ml) and brine solution (20 ml), dried over Na_2SO_4, and evaporated to dryness to yield compound (4).

Synthesis of Compound (5a): To a solution of compound (4) (1 mmol) in DCM (20 ml), oxalyl chloride (1.5 mmol) was added dropwise at 0 °C. After 5 minutes, a catalytic amount of DMF (3 drops) was added, and the reaction was stirred at RT. After completion, the reaction mixture was concentrated to remove excess oxalyl chloride under nitrogen, yielding the neat acid chloride.

The acid chloride was then dissolved in fresh DCM (25 ml), followed by the addition of triethylamine (2 mmol) at 0 °C. To this solution, 4-piperidone (1.1 mmol) was added at 0 °C, and the mixture was stirred until the reaction was complete. The reaction was then diluted with water (50 ml) and extracted with DCM (2 × 100 ml). The combined organic layer was washed with water (50 ml) and brine solution (20 ml), dried over Na_2SO_4, and evaporated to dryness. Crude products were purified by washing with diethyl ether.

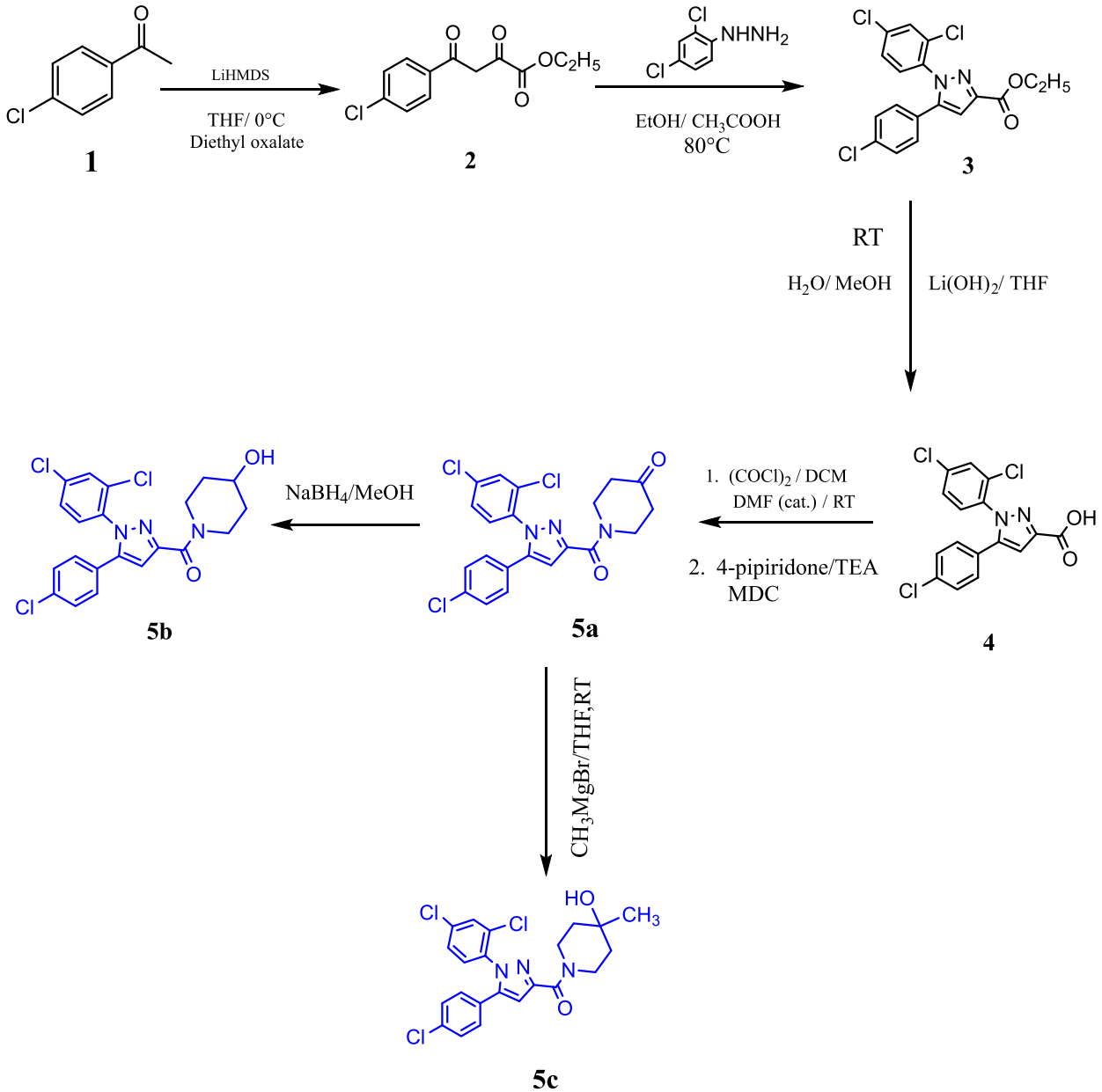

Scheme 1. Synthesis of chlorophenyl substituted pyrazalone

Synthesis of Compound (5b): Alternatively, to a solution of compound (5) (1 mmol) in methanol (20 ml), sodium borohydride (1.2 mmol) was added in portions over 5 minutes. The reaction mixture was stirred at RT for 2 hours. After completion, the reaction mixture was concentrated to remove methanol, and the residue was dissolved in water (50 ml). The aqueous solution was extracted with ethyl acetate (2×100 ml). The combined organic layer was washed with water (50 ml) and brine solution (20 ml), dried over Na_2SO_4, and evaporated to dryness. The crude product was directly used for the next step without further purification.

Synthesis of Compound (5c): To a solution of compound (5) (1 mmol) in THF (20 ml), methylmagnesium bromide (1.5 mmol) was added dropwise at 0 °C. After the addition, the reaction mass was allowed to warm to RT, and the progress was monitored by TLC. Upon completion, the mixture was quenched with saturated ammonium chloride and extracted with ethyl acetate (2 × 100 ml). The organic layer was washed with water (50 ml) and brine solution (20 ml), dried over Na_2SO_4, and evaporated to dryness. The crude product was purified by column chromatography using 230–400 silica gel.

Structural characterization of 1-(5-(4-chlorophenyl)-1-(2,4-dichlorophenyl)-1H-pyrazole-3-carbonyl) piperidin-4-one (5a)

White solid, mp 138.8 °C; % Yield: 76; ^{1}H NMR (400MHz, d_6-DMSO): δ= 7.87(d, J= 4Hz, 1H, ArH), 7.75(d, 1H, ArH), 7.62(q, 1H, ArH), 7.46(t, 2H, ArH), 7.27(t, 2H, ArH), 7.11(s, 1H, pyrazole CH), 4.18(t, 2H, -CH_2), 3.92(t, 2H, -CH_2), 2.45(t, 4H, -CH_2-CH_2); MS calcd.for $C_{21}H_{16}Cl_3N_3O_2$: 448.73, Found: 448; IR (ν cm^{-1}): 3411(O-H), 3084(Ar-H), 1722(C-C=O), 1621(N-C=O); Elem. Anal. cald (found): C: 56.21(56.20), H: 3.59(3.50), N: 9.36(9.35).

Structural characterization of (5-(4-chlorophenyl)-1-(2,4--dichlorophenyl)-1H-pyrazol-3-yl)(4-hydroxypiperidin-1-yl) methanone (5b)

Pale brown solid, mp 213.6 °C; % Yield: 85; ^{1}H NMR (400MHz, d_6-DMSO): δ= 7.75(d, 1H, ArH), 7.62(m, 1H, ArH), 7.60(m, 1H, ArH), 7.44(m, 2H, ArH), 7.25(t, 2H, ArH), 7.01(s, 1H, pyrazole CH), 4.77(d, 1H, -CH), 4.18(m, 1H, -CH), 4.03(m, 1H, -CH), 3.74(m, 1H, -OH), 3.46(m, 1H, -CH), 3.23(m, 1H, -CH), 1.78(t, 2H, -CH_2), 1.17(t, 2H, -CH_2); MS calcd. for $C_{21}H_{18}Cl_3N_3O_2$: 450.75, Found: 452.0 [M+1]; IR (ν cm^{-1}): 3429(O-H), 1612(C=O), 1384(C=C_{ring}); Elem. Anal. cald (found): C: 55.96(55.92), H: 4.03(4.01), N: 9.32(9.30).

Structural characterization of (5-(4-chlorophenyl)-1-(2,4--dichlorophenyl)-1H-pyrazol-3-yl)(4-hydroxy-4-methylpiperidin-1-yl)methanone (5c)

White solid, mp 82.8 °C; % Yield: 86; ^{1}H NMR (400MHz, $CDCl_3$): δ= 7.50(d, 1H, ArH), 7.31(d, 1H, ArH), 7.26(m, 3H, ArH), 7.15(q, J= 4Hz, 2H, ArH), 6.90(s, 1H, pyrazole CH), 4.36(m, 2H, -CH_2), 3.65(t, 1H, -OH), 3.36(t, 1H, -CH), 2.65(m, 1H, -CH), 1.71(q, 4H, -CH_2-CH_2), 1.26(s, 3H, -CH_3); MS calcd. for $C_{22}H_{20}Cl_3N_3O_2$: 464.77, Found: 466; IR (ν cm^{-1}): 3395(O-H), 2920(C-H), 1607(C=O), 1478(C=C_{ring}); Elem. Anal. cald (found): C: 56.85(56.83), H: 4.34(4.32), N: 9.04(9.02).

RESULTS AND DISCUSSION

Computational photophysical studies

The synthetic approach, outlined in Scheme 1, was carried out using the Baylis-Hillman acetate reaction. Additionally, DFT-B3LYP-6-31(G)[22] levels were utilized to determine equilibrium structures for the three dyes. Fig. 1 illustrates the optimized molecular geometry of the synthesized molecule. These computations, carried out using Gaussian-09W software, revealed predominantly planar ground state geometries, except the pyrazole group, where rotation of the piperidin-4-one groups was observed to prevent steric clashes. Notably, in dyes 5b and 5c, planarity led to short distances of 1.41 Å between carbon and piperidin-4-one. The computed Highest Occupied Molecular Orbital (HOMO) and Lowest Unoccupied Molecular Orbital (LUMO) orbitals for molecules 5a–5c are depicted in Fig. 2, showing consistent characteristics regardless of linker length. The HOMO orbital, primarily of π-character, exhibited delocalization across the entire molecule, including the chlorophenyl, supporting observations from electrochemical experiments. Conversely, the LUMO orbital, also with π-character, displayed minimal contribution from the 1-(2,4-dichlorophenyl)-1H-pyrazole groups. TDDFT calculations unveiled that the lowest excitation in all three synthesized molecules involved a charge-transfer transition predominantly of HOMO-LUMO character. In the first excited state, electron density shifted towards the opposite end of the molecule, indicating a significantly larger dipole moment compared to the ground state. Consequently, computed oscillator strengths were substantial across all molecules, with a tendency to increase with linker length, as shown in Table 1. Similarly, the absorption wavelengths showed a consistent pattern of increase with the length of the linker, aligning with the experimental absorption spectra. Nonetheless, the computed wavelengths tended to be overestimated, especially in the case of longer dyes. The expectation of this overestimation stemmed from the widely recognized tendency of traditional exchange-correlation functionals like B3LYP to underestimate energies linked to charge-transfer transitions. This disparity becomes more apparent as the distance between negative and positive charges within the charge-transfer state increases.

Table 1. Computed TD-DFT absorption wavelengths (λ_{max}) and oscillator strengths (f) of the synthesised molecules

Sample	λ_{max} (nm)	f
5a	321	0.95
5b	332	1.23
5c	334	1.28

A molecular orbital is a mathematical function employed to describe the behavior of an electron or a pair of electrons within a molecule. The HOMO and LUMO are pinpointed by the transition from occupied to unoccupied orbital occupancy. This transition typically corresponds to the change from positive to negative orbital energies, though exceptions exist. To delve deeper into the electronic properties of the molecule, various global chemical reactivity descriptor (GCRD) parameters were estimated and are given in Table 2. In basic molecular orbital theory, the HOMO energy was associated with

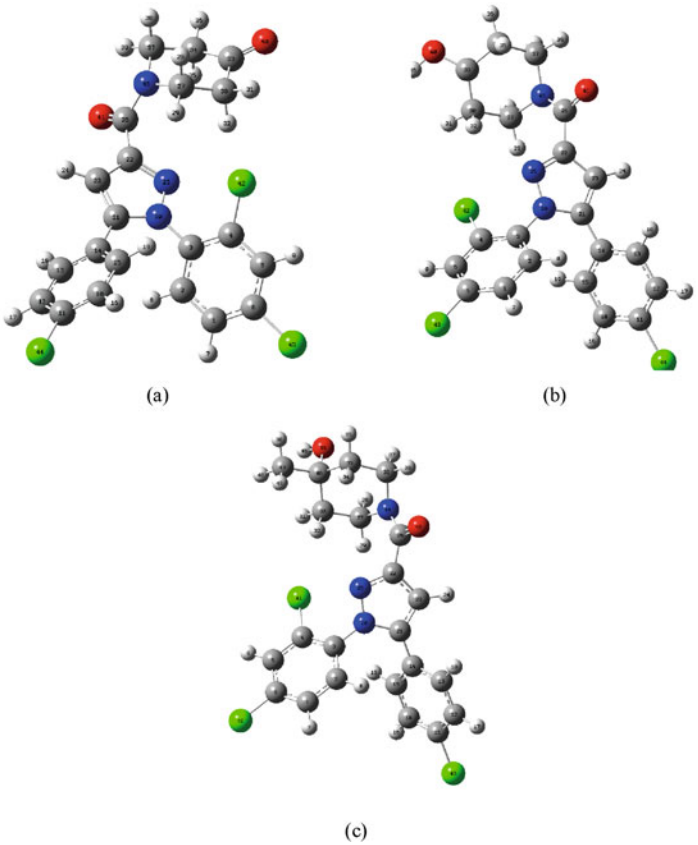

Figure 1. Optimised molecular geometry of chlorophenyl substituted pyrazalone molecules

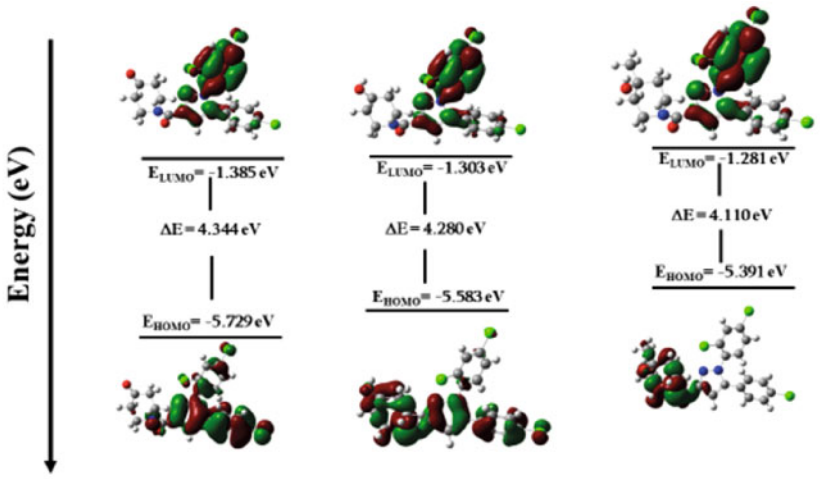

Figure 2. Frontier molecular diagram of chlorophenyl substituted pyrazalone molecule

ionization potential (Z = E_{HOMO}), and LUMO energy was associated with electron affinity (E= E_{LUMO}). The electronegativity (χ) of the synthesized molecule was estimated using the following equation based on the energy of the HOMO-LUMO[23–25].

$$\chi = \frac{Z-E}{2} \quad (1)$$

Chemical potential (μ) is expressed as

$$\mu = -\frac{Z-E}{2} \quad (2)$$

Additionally, the determination of HOMO-LUMO energies aids in comprehending the chemical stability of a molecule, quantified by a parameter called Global hardness (η). The Global hardness is computed using the equation below.

$$\eta = \frac{Z+E}{2} \quad (3)$$

The energy gap and chemical hardness are indicators of the molecule's chemical reactivity. Global hardness is inversely proportional to chemical softness (σ) and expressed.

$$\sigma = \frac{1}{2\eta} \quad (4)$$

The electrophilicity index (ω) is expressed as

$$\omega = \frac{\mu^2}{2\eta} \quad (5)$$

The electrophilicity index offers a more comprehensive depiction of global chemical reactivity as it integrates details concerning both electron transfer (chemical potential) and stability (hardness).

The μ stands for the tendency of electrons to escape from a stable system. A negative chemical potential suggests the stability of a complex, indicating its reluctance to

Table 2. The GCRD parameters of chlorophenyl substituted pyrazalone

Sample	HOMO (eV)	LUMO (eV)	ΔE (eV)	Z (eV)	E (eV)	η (eV)	χ (eV)	μ (eV)	σ (eV)	ω (eV^{-1})
5a	–5.729	–1.385	4.344	5.729	1.385	2.172	3.557	–3.557	0.230	2.913
5b	–5.583	–1.303	4.280	5.583	1.303	2.140	3.443	–3.443	0.234	2.770
5c	–5.391	–1.281	4.110	5.391	1.281	2.055	3.336	–3.336	0.243	2.708

spontaneously decompose into its elemental components. Hardness, on the other hand, serves as a gauge for the resistance to alterations in the electron distribution within a molecule. Interestingly, hardness and aromaticity share a common relationship. Studies by Parr and colleagues, as well as Zhou and Parr, have established a correlation between global hardness (both absolute and relative) and the aromaticity of various unsubstituted aromatic compounds. It appears that molecules tend to arrange themselves to maximize their hardness, reflecting their stability. Essentially, hardness denotes the ability of a chemical system to withstand the deformation of its electron cloud when subjected to minor perturbations during chemical processes. A molecule characterized by the highest energy band gap is termed as hard, while one with a narrower gap is considered soft, hence more reactive. Soft systems typically exhibit larger sizes and higher polarizability, whereas hard systems are relatively smaller and less polarizable. Local hardness provides insights into intermolecular reactivity, while global hardness offers clues about overall molecular stability. Softness, the reciprocal of hardness, complements this understanding. Electrophilicity, which pertains to the capacity of an electrophile to receive of electronic charge and resist exchanging electronic charge with its environment, sheds light on both electron transfer (chemical potential) and stability (hardness). The electrophilicity index emerges as a critical quantum chemical descriptor, particularly in evaluating the toxicity and reactivity of molecules, thus quantifying their biological activity, especially in drug-receptor interactions. Reactivity descriptors of ligands and complexes, provided in Table 2, underscore their stability through negative chemical potential values, indicating their resistance to decomposition. The observed magnitudes of chemical hardness, supported by HOMO-LUMO gap measurements, further affirm their hardness and resistance to electron cloud deformation under minor perturbations, rendering them less polarizable. Notably, the modest magnitudes of global softness rule out the possibility of their soft nature. The electrophilicity index values ω provide insights into their nucleophilic potency, intertwined with chemical potential and hardness characteristics. Overall compound 5a shows high electrophilic and stable molecule due to the substitution of piperidin-4-one linked to pyrazole molecules[26–29].

The theoretically calculated Global Chemical Reactivity Descriptors (GCRD) parameters can offer significant insights into predicting the potential adverse effects of the studied compounds. For example, the HOMO (Highest Occupied Molecular Orbital) and LUMO (Lowest Unoccupied Molecular Orbital) energies, along with the energy gap (ΔE) between them, reveal the compounds' chemical reactivity and stability. A smaller ΔE suggests higher reactivity, which might lead to unintended interactions with cellular macromolecules, potentially causing toxicity. Additionally, the electrophilicity index (ω) indicates the compound's tendency to form harmful adducts with biomolecules, such as DNA or proteins, which could result in genotoxicity or protein dysfunction. Chemical hardness (η) and softness parameters show how readily a compound undergoes chemical changes, with softer compounds potentially leading to increased off-target effects and toxicity. The chemical potential (μ) and electronegativity (χ) values provide insights into the compound's electron-accepting or electron-donating tendencies, highlighting possible undesirable reactions in biological systems. By analyzing these parameters, researchers can anticipate how compounds might interact with biological targets, predict potential toxicological issues, and guide modifications to enhance safety while maintaining efficacy.

Mulliken charge distribution

The Mulliken charge distribution analysis for the 3MSQ molecule, outlined in bar graph and represented in Fig. 3a–c, provides insights into the distribution of charges across individual atoms. Within 5a molecule, certain atoms including 1C, 2C, 3C, 4C, 6C, 11C, 13C, 15C, 21C, 26C are identified as donor atoms. Conversely, carbon atoms forming bonds with oxygen (26C, 33C) and nitrogen (22C, 37C, 27C) function as acceptors, akin to hydrogen atoms. Additionally, Chlorine (42, 43, 44) and hydrogen atoms act as acceptors within this context.

The atomic charge of Nitrogen (25N) experiences an increase in magnitude with rising solvent polarity, consistent with the behavior observed in carbon, hydrogen, nitrogen, and chlorine atoms. However, notably diverging from this trend, the atomic charge on chlorine does not follow the same pattern. Instead, the sulphur atomic charge tends to decrease as the polarity of the medium increases. This observation suggests that, within the 5a molecule, while the charges on most atoms correlate with solvent polarity, chlorine atoms exhibit a contrasting behavior, showing a decrease in atomic charge as the polarity of the medium intensifies. Such variations in Mulliken charges reflect the differing electronegativities and polarizabilities of the atoms comprising the molecules' structure, influencing their responses to changes in solvent polarity[30]. Similar results are observed for 5b and 5c molecules.

In vitro biological activity

The antifungal and antibacterial activities of synthesized pyrazolones were evaluated using various methodologies. To assess antifungal properties against *A. niger* and *C. albicans*, the serial plate dilution method was employed. Sabouraud's agar media was prepared and seeded with fungal spore suspensions, followed by the creation of wells for compound testing. Test compounds of concentration ranging from 10 μg/mL to 50 μg/mL were prepared in DMSO and incubated at 37 °C for 3–4 days to observe inhibition zones and compared with Fluconazole. For

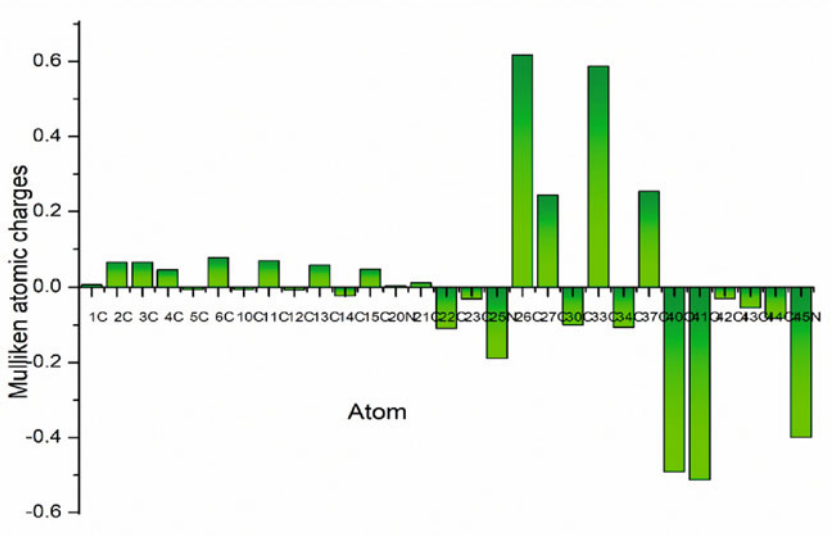

Figure 3a. Mulliken atomic charges of 5a molecule

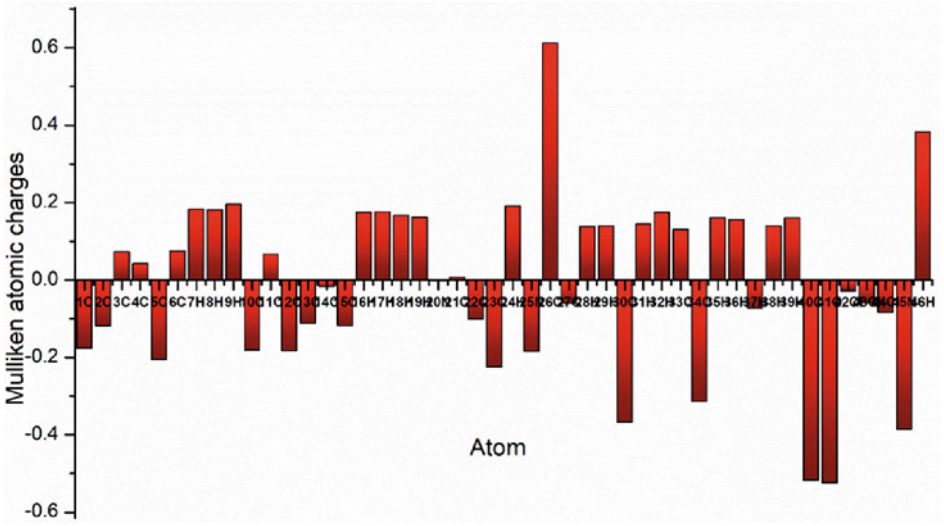

Figure 3b. Mulliken atomic charges of 5b molecule

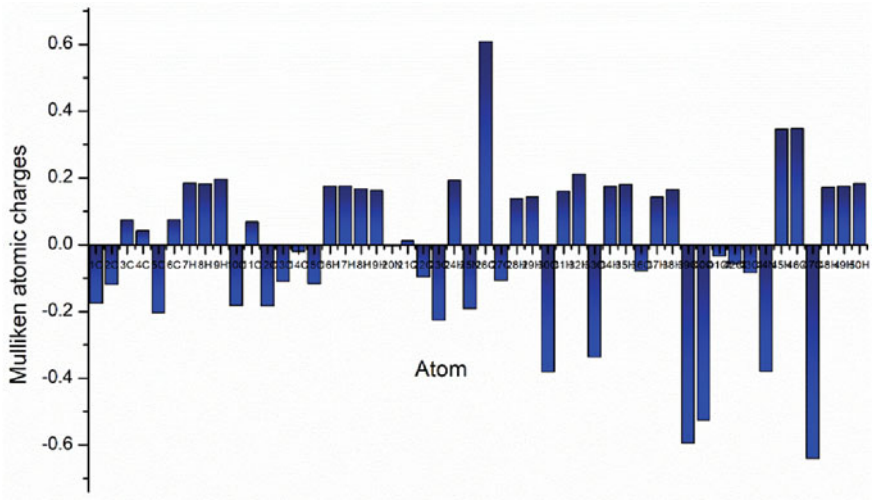

Figure 3c. Mulliken atomic charges of 5c molecule

antibacterial evaluation against *S. aureus*, *B. subtilis*, *E. coli*, and *S. typhi*, the disc diffusion method was utilized. Sterilized discs impregnated with test compounds in DMSO were placed onto nutrient agar plates seeded with bacteria. After 24 hours of incubation at 37 °C, zones of inhibition and minimum inhibitory concentrations were determined, with Ciprofloxacin used as the standard. Controls with solvent and bacterial growth were included in both experiments for comparative analysis[31].

The recently synthesized pyrazalone derivatives, featuring chlorophenyl substitution, underwent antimicrobial assessments. Remarkably, the compound demonstrated exceptional antibacterial efficacy against *S. aureus*, *B. subtilis*, *S. typhi*, and *E. coli*, as outlined in Table 3. Furthermore, the molecule displayed highly effective antifungal properties against A. niger and C. albicans, as detailed in the same table. Out of the three molecules, 5a exhibits the highest activity attributed to the

Table 3. Detail of Antimicrobial and antifungal activity

Compound	*S. aureus*	*B. subtilis*	*S. typhi*	*E. coli*	*A. niger*	*C. albicans*
5a	28	28	29	29	25	25
5a	26	27	28	26	20	24
5c	25	24	25	27	23	25
Standard	23	23	24	25	23	24
Control DMSO	0	0	0	0	0	0

Note: Standard drug: Bacteria (Ciprofloxacin); Fungal (Flucanazole) (40 µ/mL).
Compounds used: (40 µg /mL)

piperidin-4-one moiety, which mimics hydrogen in terms of steric demands at enzyme receptor sites. This presence of piperidin-4-one boosts absorption rates due to its heightened lipid solubility. The pronounced lipophilic nature of the piperidin-4-one group plays a crucial role in enhancing pharmacological activity.

In vitro antiproliferative studies

The MTT assay, a commonly used colorimetric method, serves to assess the cytotoxicity of compounds. Anti-proliferative screening of compounds was carried out against human liver carcinoma cell line (HepG2)[32]. It was found that all the compounds have excellent antiproliferative activities against HepG2 cell lines. The presence of 4-piperidone amide linkage is responsible for the high activity against HepG2 cell line. The results demonstrated that the compounds exhibited selectivity against proliferative cells while having no inhibitory effect on normal HepG2 cells. The IC50 values for the compounds are given in the Table 4.

Table 4. IC50 values of compounds

Compounds	IC_{50} (µg/mL)
5a	6
5b	20
5c	89

The increased anticancer activity of chlorophenyl pyrazolone derivatives, particularly compounds 5a, 5b, and 5c, can be explained by the functional groups present in their structures and their influence on biological mechanisms. One significant functional group is the chlorophenyl ring. The presence of chlorine atoms on the phenyl rings serves as an electron-withdrawing group, which increases the polarity and reactivity of the molecule. This enhances the compounds' ability to interact with biological targets, such as enzymes and receptors that play crucial roles in cancer cell growth. The chlorophenyl groups are known to improve the binding affinity of these molecules to cancer-related proteins, which may result in the inhibition of pathways like cell cycle progression or apoptotic resistance. Compound 5a, which has two chlorophenyl groups, shows the strongest anticancer activity with an IC50 of 6 µg/mL, compared to 5b (IC50 = 20 µg/mL) and 5c (IC50 = 89 µg/mL). The pyrazolone ring also contributes to the anticancer mechanism. The pyrazolone moiety can act as a key scaffold for interacting with proteins involved in apoptosis. This ring structure may induce apoptosis by triggering the intrinsic (mitochondrial) or extrinsic (death receptor) pathways. The chlorophenyl substitution at the 5-position of the pyrazolone ring in compound 5a may enhance its interaction with apoptotic proteins, such as caspases, leading to the efficient activation of programmed cell death in cancer cells.

Additionally, the carbonyl group (-C=O) in these compounds plays a role in generating reactive oxygen species (ROS), particularly through interactions with cellular components. Increased ROS production can lead to oxidative stress in cancer cells, causing DNA damage and lipid peroxidation. The carbonyl group, combined with the electron-withdrawing chlorophenyl rings, enhances the molecule's potential to disrupt cancer cell membranes and initiate oxidative damage, leading to cell death. The piperidine and hydroxyl groups present in compounds 5b and 5c, while contributing to the overall structure, seem to reduce the anticancer activity compared to 5a. The bulkier piperidine and hydroxyl groups may affect the compounds' ability to penetrate the cell membrane or interact efficiently with target proteins, leading to higher IC50 values. In contrast, 5a, with a less hindered structure, exhibits better cell penetration and interaction with critical cellular components, leading to its lower IC50 value.

The enhanced anticancer activity of compound 5a, compared to 5b and 5c, can be attributed to several key biological mechanisms. First, the piperidin-4-one moiety in 5a increases lipophilicity, improving cellular membrane permeability, and allowing greater intracellular concentrations of the drug. This enhances its ability to disrupt cancer cell functions such as DNA replication and protein synthesis. The piperidin-4-one group may also promote apoptosis by interacting with mitochondrial pathways or inhibiting anti-apoptotic proteins like Bcl-2.

Additionally, pyrazolone derivatives are known to inhibit cyclooxygenase-2 (COX-2), which is overexpressed in many cancers. By reducing prostaglandin production, 5a likely decreases cancer cell proliferation and inflammation more effectively than 5b or 5c. Its metal-chelating properties may further disrupt metal-dependent processes, essential for cancer cell survival. The structural features of 5a, particularly the chlorophenyl substitution, enhance its ability to interact with cancer-specific receptors or enzymes, contributing to selective cytotoxicity. This increased interaction with critical cancer pathways likely leads to cell cycle arrest and increased cancer cell apoptosis. The amide linkage in the piperidin-4-one ring may also facilitate specific receptor binding, contributing to its potency. Overall, the combination of increased lipophilicity, COX-2 inhibition, metal chelation, and enhanced ROS generation explains the superior anticancer activity of compound 5a. These mechanisms make it a promising candidate for further exploration as an anticancer agent, particularly in targeting liver carcinoma cells.

The superior anticancer activity of compound 5a is attributed to the presence of two chlorophenyl groups and a pyrazolone ring, which enhance the molecule's

ability to induce apoptosis, generate ROS, and interact with key biological targets. The carbonyl group further contributes to the oxidative stress in cancer cells, while the structural simplicity of 5a, compared to 5b and 5c, ensures more effective anticancer activity.

CONCLUSIONS

In this study, we synthesized chlorophenyl-substituted pyrazolone derivatives, thoroughly confirming their physicochemical properties through ^{1}H-NMR, FT-IR, and LC-MS data analysis. Employing computational techniques, the photophysical characteristics of the compounds were estimated. Through DFT-B3LYP-6-31G(d) basis set calculations, optimized molecular geometries, HOMO-LUMO distributions, and MESP plots for the synthesized molecules were estimated. Additionally, absorption spectra and oscillator factors were estimated using the TD-DFT method. By leveraging theoretical HOMO-LUMO values, we derived global chemical reactive descriptor parameters, revealing the synthesized molecule's strong electrophilic nature, indicative of its reactivity albeit relatively lower stability. Through DFT computational studies, electron-deficient sites in 5a were pinpointed, offering potential avenues for drug design in biological applications. Subsequent examination of the synthesized molecule's in vitro antimicrobial, antifungal, and antioxidant activities underscored its significant biological potential. Among the three chlorophenyl-substituted pyrazolone derivatives 5a, 5b, and 5c compound 5a exhibited the highest antibacterial, antifungal, and antiproliferative activities. This enhanced biological performance can be attributed to the presence of the piperidin-4-one moiety, which increases lipophilicity, facilitating better cell membrane permeability and absorption. Additionally, the lower HOMO-LUMO gap of 5a (4.344 eV) indicates higher chemical reactivity, making it more effective at interacting with biological targets. In contrast, compound 5b, which contains a 4-hydroxy-4-methylpiperidine moiety, showed moderate activity, likely due to its slightly higher HOMO-LUMO gap (4.280 eV) and the steric hindrance caused by the methyl group, which may reduce interaction with biological molecules. Compound 5c, with a 4-hydroxypiperidine moiety, displayed the lowest activity, potentially due to its higher HOMO-LUMO gap (4.110 eV) and lower electrophilicity, which could reduce its reactivity and cellular uptake. These findings suggest that the structural differences at the piperidine ring play a crucial role in the biological activity of the compounds. Future research should focus on optimizing these structural features, especially the piperidine ring, to improve reactivity and lipophilicity. Further biological testing and toxicological studies are necessary to assess the therapeutic potential of these compounds. Moreover, antiproliferative studies demonstrated promising anticancer activity for the synthesized molecules. These findings position the synthesized molecule as a valuable asset in drug design, particularly in the realm of anticancer applications. Overall, our results suggest promising prospects for the synthesized molecules in future anticancer therapeutics.

ACKNOWLEDGMENTS

Authors are grateful to King Saud University, Riyadh, Saudi Arabia for funding the work through Researchers Supporting Project No. (RSP2024R359).

LITERATURE CITED

1. Arora, P., Arora, V., Lamba, H.S., Wadhwa, D. (2012). Importance of heterocyclic chemistry: A review. *IJPSR*, 3.

2. Martins, P., Jesus, J., Santos, S., Raposo, L.R., Roma-Rodrigues, C., Baptista, P.V., Fernandes, A.R. (2015). Heterocyclic anticancer compounds: Recent advances and the paradigm shift towards the use of nanomedicine's toolbox. *Molecules*, 20. DOI: 10.3390/molecules200916852.

3. Eftekhari-Sis, B., Zirak, M., Akbari, A. (2013). Arylglyoxals in synthesis of heterocyclic compounds. *Chem. Rev*. 113. DOI: 10.1021/cr300176g.

4. Alamgir, A.N.M. (2018). Secondary metabolites: Secondary metabolic products consisting of C and H; C, H, and O; N, S, and P elements; and O/N heterocycles. Progress in Drug Research. DOI: 10.1007/978-3-319-92387-1_3.

5. Bhambhani, S., Kondhare, K.R., Giri, A.P. (2021). Diversity in chemical structures and biological properties of plant alkaloids. *Molecules*, 26. DOI: 10.3390/molecules26113374.

6. Alamgir, A.N.M. (2018). Phytoconstituents—Active and inert constituents, metabolic pathways, chemistry and application of phytoconstituents, primary metabolic products, and bioactive compounds of primary metabolic origin. Progress in Drug Research. DOI: 10.1007/978-3-319-92387-1_2.

7. Lang, D.K., Kaur, R., Arora, R., Saini, B., Arora, S. (2020). Nitrogen-containing heterocycles as anticancer agents: An overview. *Anticancer Agents Med. Chem*. 20. DOI: 10.2174/1871520620666200705214917.

8. Bhardwaj, N., Pathania, A., Kumar, P. (2020). Naturally available nitrogen-containing fused heterocyclics as prospective lead molecules in medicinal chemistry. Current Traditional Medicine, 7. DOI: 10.2174/2215083805666190613125700.

9. Faisal, M., Saeed, A., Hussain, S., Dar, P., Larik, F.A. (2019). Recent developments in synthetic chemistry and biological activities of pyrazole derivatives. *J. Chem. Sci.* 131. DOI: 10.1007/s12039-019-1646-1.

10. Karrouchi, K., Radi, S., Ramli, Y., Taoufik, J., Mabkhot, Y.N., Al-Aizari, F.A., Ansar, M. (2018). Synthesis and pharmacological activities of pyrazole derivatives: A review. *Molecules*, 23. DOI: 10.3390/molecules23010134.

11. Ansari, A., Ali, A., Asif, M., Shamsuzzaman, S. (2017). Review: Biologically active pyrazole derivatives. *J. Chem.* 41, 16–41. DOI: 10.1039/C6NJ03181A.

12. Chauhan, S., Paliwal, S., Chauhan, R. (2014). Anticancer activity of pyrazole via different biological mechanisms. *Synth. Commun.* 44. DOI: 10.1080/00397911.2013.837186.

13. Abrigach, F., Touzani, R. (2016). Pyrazole derivatives with NCN junction and their biological activity: A review. *Med. Chem.* (Los Angeles), 6. DOI: 10.4172/2161-0444.1000359.

14. Kumar, V., Kaur, K., Gupta, G.K., Sharma, A.K. (2013). Pyrazole containing natural products: Synthetic preview and biological significance. *Eur. J. Med. Chem*. 69, DOI: 10.1016/j.ejmech.2013.08.053.

15. Mantzanidou, M., Pontiki, E., Hadjipavlou-Litina, D. (2021). Pyrazoles and pyrazolines as anti-inflammatory agents. *Molecules,* 26. DOI: 10.3390/molecules26113439.

16. Ravindar, L., Hasbullah, S.A., Rakesh, K.P., Hassan, N.I. (2023). Pyrazole and pyrazoline derivatives as antimalarial agents: A key review. *Europ. J. Sci.* 183. DOI: 10.1016/j.ejps.2022.106365.

17. Britton, J., Jamison, T.F. (2017). A unified continuous flow assembly-line synthesis of highly substituted pyrazoles and pyrazolines. Angewandte Chemie - International Edition, 56. DOI: 10.1002/anie.201704529.

18. Kumar, S., Bawa, S., Drabu, S., Kumar, R., Gupta, H. (2009). Biological activities of pyrazoline derivatives - A recent development. Recent Pat. Antiinfect. Drug Discov., 4. DOI: 10.2174/157489109789318569.

19. Varghese, B., Al-Busafi, S.N., Suliman, F.O., Al-Kindy, S.M.Z. (2017). Unveiling a versatile heterocycle: Pyrazoline - A review. RSC Adv. 7. DOI: 10.1039/c7ra08939b.

20. van Alphen, J. (1943). Pyrazolines and their rearrangement to form pyrazoles. II. (Pyrazole and pyrazoline derivatives, IV). Recueil des Travaux Chimiques des Pays-Bas, 62. DOI: 10.1002/recl.19430620713.

21. Faidallah, H.M., Khan, K.A., Rostom, S.A.F., Asiri, A.M. (2013). Synthesis and in vitro antitumor and antimicrobial activity of some 2,3-diaryl-7-methyl-4,5,6,7-tetrahydroindazole and 3,3a,4,5,6,7-hexahydroindazole derivatives. *J. Enzyme Inhib. Med. Chem.* 28. DOI: 10.3109/14756366.2011.653354.

22. M.J. Frisch, G.W., Trucks, H.B., Schlegel, G.E., Scuseria, M.A., Robb, J.R., Cheeseman, G., Scalmani, V., Barone, B., Mennucci, G.A., Petersson, H., Nakatsuji, M., Caricato, X., Li, H.P., Hratchian, A.F., Izmaylov, J., Bloino, G., Zheng, J.L., Sonnenberg, M., Hada, M., Ehara, K., Toyota, R., Fukuda, J., Hasegawa, M., Ishida, T., Nakajima, Y., Honda, O., Kitao, H., Nakai, T., Vreven, J.A., Montgomery Jr., J.E., Peralta, F., Ogliaro, M., Bearpark, J.J., Heyd, E., Brothers, K.N., Kudin, V.N., Staroverov, T., Keith, R., Kobayashi, J., Normand, K., Raghavachari, A., Rendell, J.C., Burant, S.S., Iyengar, J., Tomasi, M., Cossi, N., Rega, J.M., Millam, M., Klene, J.E., Knox, J.B., Cross, V., Bakken, C. Adamo, J., Jaramillo, R., Gomperts, R.E. Stratmann, O. Yazyev, A.J. Austin, R. Cammi, C. Pomelli, J.W. Ochterski, R.L., Martin, K., Morokuma, V.G., Zakrzewski, G.A., Voth, P., Salvador, J.J., Dannenberg, S., Dapprich, A.D., Daniels, O., Farkas, J.B., Foresman, J.V., Ortiz, J., Cioslowski, D.J,. Fox, Gaussian-09, Revision B.01, Gaussian, Inc, Wallingford, CT, 2010.

23. Parr, R.G., Szentpály, L.V., Liu, S. (1999). Electrophilicity index. *J. Am. Chem. Soc*. 121. DOI: 10.1021/ja983494x.

24. Pearson, R.G. (2005). Chemical hardness and density functional theory. *J. Chem. Sci*. 117. DOI: 10.1007/BF02708340.

25. Sexton, K. (1997). Sociodemographic aspects of human susceptibility to toxic chemicals: Do class and race matter for realistic risk assessment? Environ. Toxicol. Pharmacol., DOI: 10.1016/S1382-6689(97)10020-5.

26. Maridevarmath, C.V., Naik, L., Negalurmath, V.S., Basanagouda, M., Malimath, G.H. (2019). Synthesis, characterization and photophysical studies on novel benzofuran-3-acetic acid hydrazide derivatives by solvatochromic and computational methods. *J. Mol. Struct.* 1188. DOI: 10.1016/j.molstruc.2019.03.063.

27. Naik, L., Thippeswamy, M.S., Praveenkumar, V., Malimath, G.H., Ramesh, D., Sutar, S., Savanur, H.M., Gudennavar, S.B., Bubbly, S.G. (2023). Solute-solvent interaction and DFT studies on bromonaphthofuran 1,3,4-oxadiazole fluorophores for optoelectronic applications. *J. Mol. Graph. Model*. 118. DOI: 10.1016/j.jmgm.2022.108367.

28. Walki, S., Naik, L., Savanur, H.M., K.C., Y., Naik, S., M.K., R., Malimath, G.H., Mahadevan, K.M. (2020). Design of new imidazole-derivative dye having donor-π-acceptor moieties for highly efficient organic-dye-sensitized solar cells. Optik (Stuttg), 208. DOI: 10.1016/j.ijleo.2019.164074.

29. Thippeswamy, M.S., Naik, L., Maridevarmath, C.V., Malimath, G.H. (2021). A comprehensive study on photophysical and electrochemical properties of novel D-π-A thiophene substituted 1,3,4-oxadiazole derivatives for optoelectronic applications: A computational and experimental approach. *Chem. Phys.* 550. DOI: 10.1016/j.chemphys.2021.

30. C. Fonseca Guerra, J.W. Handgraaf, E.J. Baerends, F.M. Bickelhaupt, Voronoi Deformation Density (VDD) Charges: Assessment of the Mulliken, Bader, Hirshfeld, Weinhold, and VDD Methods for Charge Analysis. *J. Comput. Chem*. 25 (2004). DOI: /10.1002/jcc.10351.

31.

32. Bandna, C. (2013). Antibacterial Effect of Garlic (Allium Sativum) and Ginger (Zingiber Officinale) Against Staphylococcus Aureus, Salmonella Typhi, Escherichia Coli and Bacillus Cereus. *J. Microbiol. Biotechnol. Food Sci.* 2.

33. Jiang, Q., Yang, M., Qu, Z., Zhou, J., Zhang, Q. (2017). Resveratrol enhances anticancer effects of paclitaxel in HepG2 human liver cancer cells. *BMC Complement. Altern. Med*. 17. DOI: 10.1186/s12906-017-1956-0.